Acta Geotechnica
https://doi.org/10.1007/s11440-023-02174-y

RESEARCH PAPER

A strain-hardening macro-element model for pile groups under vertical–horizontal-moment loading

Chiara Iodice[1] · Maria Iovino[2] · Raffaele Di Laora[1] · Luca de Sanctis[2] · Alessandro Mandolini[1]

Received: 16 May 2023 / Accepted: 27 November 2023

Abstract
Pile foundations supporting wind turbines, silos, elevated water tanks or bridge piers are frequently subjected to multi-component loads, which may lead to significant rotations and settlements compromising the safe operation of the structure. The prediction of these displacements is of major concern and can be easily carried out using force-resultants plasticity models, also referred to as 'macro-elements', stemming from the idea of describing the foundation behaviour by a single upscaled constitutive relationship between generalized forces and displacements. When properly formulated, they can reproduce key aspects of the mechanical response of the foundation at low computational cost as compared to numerical analysis. To this end, a new macro-element for pile groups formulated in the classical framework of strain-hardening elasto-plasticity is presented and discussed. The required model parameters can be calibrated by closed-form equations and additional few data of numerical and/or experimental nature. The proposed mathematical framework is finally validated against the results of centrifuge tests and 3D finite element analyses.

Keywords Failure surface · Hardening rule · Macro-element · Pile foundations

1 Introduction

The large demand of tall, slender structures from energy industry has led to new research in the field of foundations under extreme loading. In particular, foundation caissons and mono-piles of unprecedented sizes are being contemplated to accommodate large, multi-component loads including inclined actions and moments. In this framework, the analysis of the soil–foundation–structure interaction is rather challenging, pushing designers towards complex numerical analysis. Actually, numerical methods require high user expertise, including the selection of appropriate constitutive models of soil behaviour and the calibration of the pertinent parameters. Further, due to the considerable volumes of surrounding and supporting soil involved in these models, high computational effort is demanded. Recently, there has been considerable interest in the development of alternative approaches like force-resultant plasticity models—or macro-elements (MEs)—in which the behaviour of the soil–foundation system is described by a unique constitutive law relating generalized force and displacement variables. The advantage of this approach over the so-called direct method is manifold as it can be easily coupled to any finite element (FE) structural model to analyse quite complex soil–structure interaction problems at low computational cost. The idea to adapt the theory of plasticity to the macroscale of the soil–foundation system dates back to the pioneers works by Roscoe and Schofield [33] and Schotman [35] on shallow foundations under static loading. Since then, a number of ME models have been proposed for circular footings on sand [18, 28], spudcan foundations [20, 27], skirted or suction caissons on clay [4, 5, 14] and deep-seated foundations of historical towers [26, 30]. Macro-element formulations capable to account for cyclic/dynamic loading effects are also available [6, 10, 12, 19, 34].

While many ME models are available for shallow foundations, the problem of pile groups has received much less attention and the very few works available on the topic have mainly concentrated on isolated piles [15, 25, 29].

✉ Raffaele Di Laora
raffaele.dilaora@unicampania.it

[1] University of Campania 'Luigi Vanvitelli', Aversa, Italy

[2] University of Napoli Parthenope, Naples, Italy

Published online: 17 February 2024

Gorini and Callisto [17] have proposed an inertial ME for pile groups, formulated in the context of hyper-plasticity, consisting in a multi-surface constitutive law with kinematic hardening derived within a rigorous thermodynamic framework. A different approach is pursued in this work, which allows for both manageable implementation and easy model parameters calibration. This novel ME for pile groups is formulated within the framework of isotropic strain-hardening elasto-plasticity by adapting the mathematical model by Nova and Montrasio [28] to include the key features of the behaviour of pile foundations.

The model is aimed at calculating the drained or undrained response of pile groups in terms of vertical and horizontal displacement as well as rotation to any arbitrary combination and temporal sequence of vertical, horizontal and moment loads. There is no limitation about the pile group layout and the history of loads acting upon the foundation, provided that the plane containing the load resultant does not change over time.

2 Formulation of ME equations

2.1 Proposed model

The principal concept adopted here is that for any load increment, the corresponding work-conjugated displacement always consists of an elastic recoverable part, ruled by the elastic stiffness matrix, while the development of the plastic component occurs only when load vector lies upon the yield surface and the load increment points outward. The shape of this surface is assumed constant, while its size varies homothetically with respect to the axes origin; for unloading states the yield surface remains fixed, with an internal state variable keeping memory of the last surface size, allowing to consider the past loading history. The yield surface evolves as function of the plastic displacement vector through a specific hardening law, until reaching the failure surface. To allow a realistic displacement pattern for the pile group, a non-associated flow rule is adopted. The complete formulation of the ME requires thus four elements: (1) the elastic stiffness matrix; (2) the yield and failure loci; (3) the hardening law; (4) the plastic potential (Fig. 1).

The closed-form equation of the yield and failure loci in the force space as well as the expression of the plastic potential are among the novel contributions of this work. The formers are derived by combining an exact solution in the axial load-moment plane based on theorems of limit analysis [8] and an approximate expression for failure surfaces in planes parallel to the axial load-horizontal load plane [9, 16, 22].

The use of the proposed ME requires the calibration of a few parameters, most of which are already necessary in routine design, such as the axial, horizontal and moment capacities of the pile group and the stiffness matrix terms. The calibration of the remaining parameters would require either experimental or numerical data, and a specific procedure to select appropriate values is also suggested in the ensuing. The prediction capability of the proposed model is successfully checked against data from centrifuge tests in soft clay under axial-moment loads [7] and rigorous numerical analyses carried out on small groups of piles under multi-component loads [32].

2.2 Mathematical formulation

The macro-element formulation for pile groups under monotonic loading presented herein relies on the classical theory of isotropic strain-hardening plasticity. In principle, the problem at the microscale of the volume element is adapted to the macroscale of the soil–foundation system, replacing the stress and deformation tensors by the resultant force, $\boldsymbol{V}$, and the corresponding displacement, $\boldsymbol{v}$, vectors with respect to which an isotropic-hardening elastoplastic law in rate form is formulated:

$$\begin{aligned} \boldsymbol{V} &= \begin{Bmatrix} Q \\ H \\ M \end{Bmatrix} \\ \boldsymbol{v} &= \begin{Bmatrix} w \\ u \\ \theta \end{Bmatrix} \\ \mathrm{d}\boldsymbol{V} &= \boldsymbol{K}\mathrm{d}\mathbf{v} \end{aligned} \tag{1}$$

where Q, H and M are the vertical, horizontal and the moment loads acting on the top of the foundation, w, u and θ are the work-conjugated displacements (vertical and horizontal) and rotations, and $\boldsymbol{K}$ is the tangent stiffness matrix of the pile group.

The total incremental displacement of the foundation is decomposed into the elastic, $\mathrm{d}\boldsymbol{v}^e$, and the plastic, $\mathrm{d}\boldsymbol{v}^p$, parts:

$$\mathrm{d}\boldsymbol{v} = \mathrm{d}\boldsymbol{v}^e + \mathrm{d}\boldsymbol{v}^p \tag{2}$$

The elastic displacement increment, $\mathrm{d}\boldsymbol{v}^e$, occurs for any change in load on the foundation. Hooke's law establishes the relationship between the recoverable displacements and the load increments:

$$\mathrm{d}\boldsymbol{V} = \boldsymbol{K}^e\mathrm{d}\boldsymbol{v}^e = K^e(\mathrm{d}\boldsymbol{v} - \mathrm{d}\boldsymbol{v}^p) \tag{3}$$

where $\boldsymbol{K}^e$ is the elastic stiffness matrix.

The boundary of the elastic domain is the yield surface, which is mathematically described as follows:

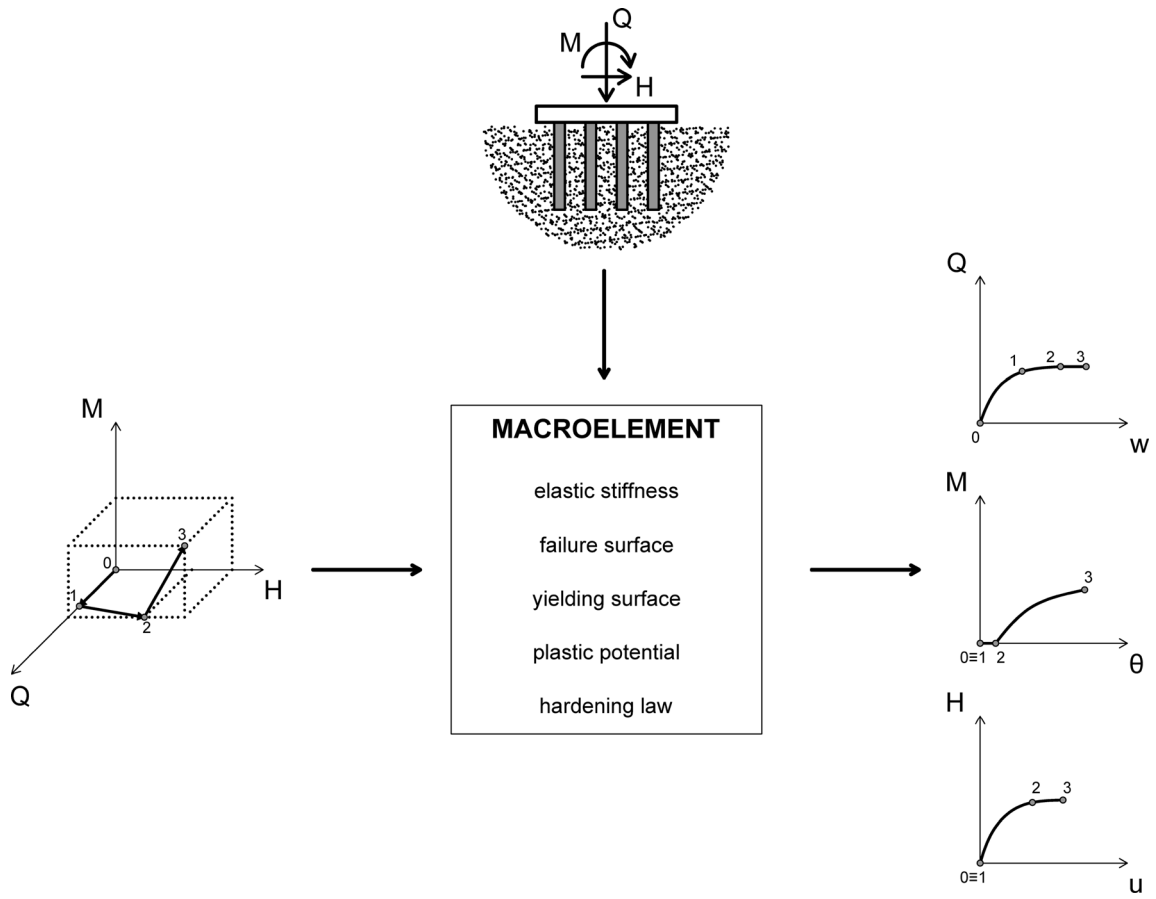

Fig. 1 Problem under investigation

$$f(\boldsymbol{V}, \rho_c) = 0 \tag{4}$$

where ρ_c is a state variable, function of the loading history of the system, which regulates the size of the surface. The yield surface is characterized by the same shape as the failure locus, the latter corresponding to $\rho_c = 1$. The function ρ_c and the incremental plastic displacements are linked through the hardening law, so that:

$$\rho_c = \rho_c(\boldsymbol{v}^p) \tag{5}$$

The plastic deformation increment occurs only when the actual load state, $\boldsymbol{V}$, lies on the yield surface and $\mathrm{d}\boldsymbol{V}$ is directed outwards. In this case, the new load state, $\boldsymbol{V} + \mathrm{d}\boldsymbol{V}$, must still lie on the (new) yielding surface, function of $\rho_c + \mathrm{d}\rho_c$. This can be obtained by imposing the so-called consistency condition:

$$f(\boldsymbol{V}, \rho_c) = 0; \quad \mathrm{d}f = \left(\frac{\partial f}{\partial \boldsymbol{V}}\right)^T \mathrm{d}\boldsymbol{V} + \frac{\partial f}{\partial \rho_c}\mathrm{d}\rho_c = 0 \tag{6}$$

In order to calculate the plastic deformations, it is postulated that there is a plastic potential function $g(\boldsymbol{V})$ such that:

$$d\boldsymbol{v}^p = \Lambda \frac{\partial g}{\partial \boldsymbol{V}} \tag{7}$$

where Λ is the plastic multiplier, a non-negative scalar quantity defining the magnitude of the plastic displacement increment. Instead, the direction of the latter is only function of the shape of the plastic potential and is expressed by its gradient. The consistency condition [Eq. (6)] together with the flow rule [Eq. (7)] gives:

$$\left(\frac{\partial f}{\partial \boldsymbol{V}}\right)^T \mathrm{d}\boldsymbol{V} + \Lambda \frac{\partial f}{\partial \rho_c}\left(\frac{\partial \rho_c}{\partial \boldsymbol{v}^p}\right)^T \frac{\partial g}{\partial \boldsymbol{V}} = 0 \tag{8}$$

which allows the calculation of the plastic multiplier as:

$$\Lambda = -\frac{\left(\frac{\partial f}{\partial \boldsymbol{V}}\right)^T}{\frac{\partial f}{\partial \rho_c}\left(\frac{\partial \rho_c}{\partial \boldsymbol{v}^p}\right)^T \frac{\partial g}{\partial \boldsymbol{V}}}\mathrm{d}\boldsymbol{V} \tag{9}$$

The aforementioned constituents have been formulated to account for the peculiarities of pile group behavior using appropriate constitutive equations, as thoroughly discussed in the subsequent sections.

2.3 Elastic stiffness parameters

The elastic relationship between the load increments and the corresponding elastic displacements is given by Eq. (3). The elastic stiffness matrix of a pile group can be put in the form:

$$\boldsymbol{K}^e = \begin{bmatrix} K_{\mathrm{v}} & 0 & 0 \\ 0 & K_h & K_{\mathrm{hm}} \\ 0 & K_{\mathrm{mh}} & K_m \end{bmatrix} \tag{10}$$

where K_{v}, K_h, $K_{\mathrm{hm}} = K_{\mathrm{mh}}$ and K_m are the vertical, swaying, cross swaying-rotational and rotational stiffnesses of the pile group, respectively. Such quantities can be evaluated through the interaction factors method [3, 31] or by numerical models. In this regard, some suggestions are provided in Sect. 3.

2.4 Failure and yield loci

The evaluation of the pile group bearing capacity under vertical, horizontal and moment loads can be conveniently carried out employing interaction diagrams. With reference to the (Q, M) plane, the closed-form solution proposed by Di Laora et al. [8] is plotted in Fig. 2 for a row of four equally spaced, identical piles. Note that, since the domain is symmetric with respect to the x-axis, only the portion for $M \geq 0$ is shown. The failure locus for vertical eccentric loads can be reasonably derived by approximating the boundary of this domain with a parabola passing through the points:

(1) (Q_{c}, 0), where Q_{c} is the bearing capacity of the pile group in compression;
(2) (Q_t, 0,), where Q_t is the bearing capacity of the pile group in uplift;
(3) (($Q_{\mathrm{c}} + Q_t$)/2, $M_{\max}$), where $M_{\max}$ is the moment capacity of the pile group.

By imposing such conditions, the following equation is obtained [21]:

$$\left|\frac{M}{M_{\max}}\right| = -4\frac{(Q - Q_{\mathrm{c}})(Q - Q_t)}{(Q_{\mathrm{c}} - Q_t)^2} \tag{11}$$

As outlined in Di Laora et al. [9], any section of the failure locus in planes parallel to (Q, H) can be reasonably approximated through a trapezium, as shown in Fig. 3 for $M = 0$. In this case, the inclined side of the trapezium connects the points of coordinates (Q_{c}, H_{c}) and (Q_t, H_t), where H_{c} and H_t are the horizontal capacity of the pile group calculated at Q_{c} and Q_t, respectively; the equation of the inclined line is therefore:

$$H = H_t + \frac{H_{\mathrm{c}} - H_t}{Q_{\mathrm{c}} - Q_t}(Q - Q_t) = H_t + i_h(Q - Q_t) \tag{12}$$

The need for a smooth function in the proposed mathematical formulation led to the choice of the Granville egg to approximate the shape of the target domain in the (Q, H) plane. The graphical construction of this function is explained in the following.

Consider a circle with centre C and radius $r = CP$, a point A on the x-axis and a line t parallel to the y-axis (Fig. 4). For any point $P = (x_P, y_P)$ lying on the circumference, the segment AP intersects line t in point $T = (x_T, y_T)$. Point Q, with coordinates (x_P, y_T), belongs to the Granville egg, which can be obtained graphically by repeating this operation for any point along the circumference.

From Fig. 4, it is easy to verify that the equation of the Granville egg may be expressed as function of the angle ω as:

$$\begin{cases} x_Q = x_P = b + r\cos\omega \\ y_Q = y_T = a\tan\omega = \dfrac{ar\sin\omega}{d + a - r\cos\omega} \end{cases} \tag{13}$$

where b is the abscissa of point C, a is the distance between point A and line t, while d is the distance between point C and line t. Alternatively, the Cartesian form may be obtained by manipulating Eq. (13) as:

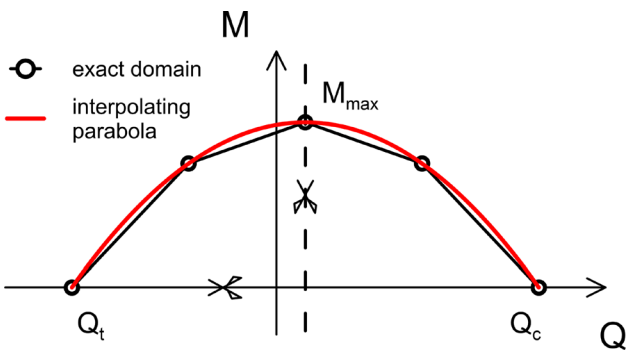

Fig. 2 Failure locus for $H = 0$: exact and approximate interaction diagrams

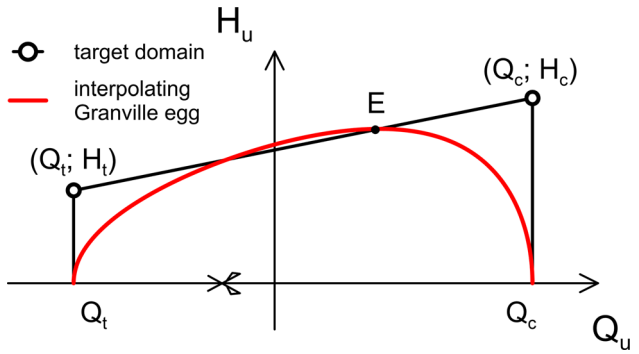

Fig. 3 Fitting of the Granville egg to the target domain in the (Q, H) plane

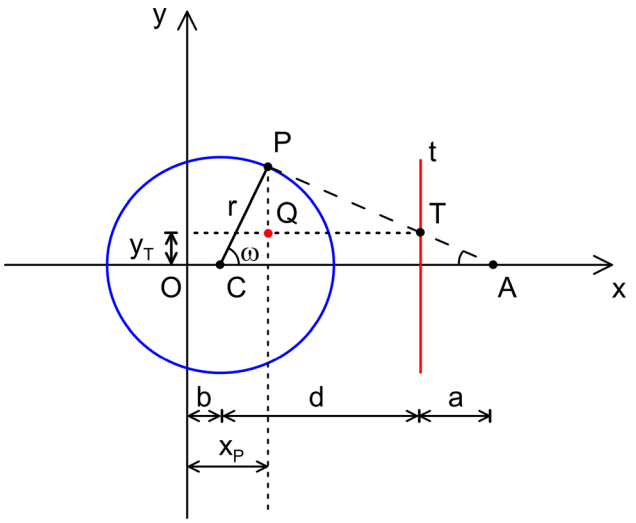

Fig. 4 Construction of the Granville egg

$$y^2 = \frac{a^2\left[r^2 - (x-b)^2\right]}{\left[(d+a) - (x-b)\right]^2} \tag{14}$$

Regarding the calibration of parameters a, b, d and r which provide a good fit to the failure interaction diagram in the (Q, H) plane for $M = 0$, the following conditions are imposed (Fig. 3):

(1) Passage through point $(Q_c, 0)$;
(2) Passage through point $(Q_t, 0)$;
(3) Passage through a peculiar point E, lying on the inclined side of the trapezium, with coordinates $(Q_E, H_E) = (Q_t + 2\beta R,\ H_t + 2i_h\beta R)$, where parameter β is a dimensionless position indicating the location of the function's maximum and $r = R = (Q_c - Q_t)/2$.
(4) Horizontal tangent at $Q = Q_E$, i.e. $H_E = H_{max}$.

Such conditions give rise to the following expressions for the egg parameters for $M = 0$:

$$\begin{cases} b = \dfrac{Q_c + Q_t}{2} \\ r = R = \dfrac{Q_c - Q_t}{2} \\ a = 2\dfrac{H_t + 2i_h\beta R}{2\beta - 1}\sqrt{\beta(1-\beta)} \\ d = \dfrac{R}{2\beta - 1} - a \end{cases} \tag{15}$$

The position of point E controls the shape of the egg. It is suggested to take:

$$\begin{cases} \beta = \dfrac{1 + 2\psi}{2(1+\psi)} \\ \psi = 1 - \dfrac{H_t}{H_c} \end{cases} \tag{16}$$

Note that β varies monotonically within the range [0.5, 0.75]. It is equal to 0.5 when the two lateral capacities are identical and to 0.75 when the collapse domain becomes a triangle, that is for $H_t = 0$. Also, the Granville egg is defined only for H_c strictly larger than H_t; when H_t tends to H_c, the egg approaches an ellipse.

The equation of the Granville egg approximating the failure locus in the (Q, H) plane can be therefore cast in the form:

$$\left(\frac{H}{H_{max}}\right)^2 = \frac{4\beta(1-\beta)\left[\left(\frac{Q-b}{R}\right)^2 - 1\right]}{\left[(2\beta - 1)\left(\frac{Q-b}{R}\right) - 1\right]^2} \tag{17}$$

Equations (11) and (17) are derived for $H = 0$ and $M = 0$, respectively. For any value of the external moment, it is possible to use Eq. (11) to determine the corresponding Q_1 and Q_2 on the parabola as:

$$\begin{aligned} Q_1 &= \frac{Q_c + Q_t}{2} - R\sqrt{1 - \frac{M}{M_{max}}} \\ Q_2 &= \frac{Q_c + Q_t}{2} + R\sqrt{1 - \frac{M}{M_{max}}} \end{aligned} \tag{18}$$

which bound the actual range of variation for Q in Eq. (12) to calculate the interaction domain in the (Q, H) plane for $M \neq 0$:

$$\begin{aligned} H_1 &= H_t + i_h(Q_1 - Q_t) \\ H_2 &= H_t + i_h(Q_2 - Q_t) \end{aligned} \tag{19}$$

This failure domain can be sill interpolated by the Granville egg updating Eqs. (15) and (16) as follows:

$$\begin{cases} b = \dfrac{Q_c + Q_t}{2} \\ r = \dfrac{Q_2 - Q_1}{2} = R\sqrt{1 - \dfrac{M}{M_{max}}} \\ a = 2\dfrac{H_t + i_h[R + r(2\beta - 1)]}{2\beta - 1}\sqrt{\beta(1-\beta)} \\ d = \dfrac{r}{2\beta - 1} - a \end{cases} \tag{20}$$

where

$$\begin{cases} \beta = \dfrac{1 + 2\psi}{2(1+\psi)} \\ \psi = 1 - \dfrac{H_1}{H_2} = \dfrac{(H_c - H_t)\sqrt{1 - \dfrac{M}{M_{max}}}}{\dfrac{H_c + H_t}{2} + \dfrac{H_c + H_t}{2}\sqrt{1 - \dfrac{M}{M_{max}}}} \end{cases} \tag{21}$$

Equations (20) and (21) clearly simplify to Eqs. (15) and (16) for $M = 0$, at which $r = R$. Substituting Eqs. (19) into (17) yields to:

$$f(\boldsymbol{V}) = \frac{\begin{array}{c} H^2\left[R\sqrt{1-\frac{M}{M_{\max}}} - (2\beta-1)(Q-b)\right]^2 + 4\beta(\beta-1)\cdot \\ \left[R^2\left(1-\frac{M}{M_{\max}}\right) - (Q-b)^2\right]\left\{H_{\max} + i_h R(2\beta-1)\left[\sqrt{1-\frac{M}{M_{\max}}} - 1\right]\right\}^2 \end{array}}{(2\beta-1)^2} = 0 \tag{22}$$

which is the explicit expression of the 3D failure locus (Fig. 5). Noteworthy, it is completely defined by only 5 parameters, (Q_c, Q_t, H_c, H_t, M_{max}), which can be easily determined by hand calculation. As a side comment, such equation may be conveniently used in routine engineering for ultimate limit state checks of pile foundations when subjected to the contemporary presence of the three load components.

The failure domain equation can be also written in a dimensionless form as:

$$f(\hat{\boldsymbol{V}}) = \frac{\begin{array}{c} h^2\left\{\lambda_Q\sqrt{1-m} + (2\beta-1)[2(1-q) - \lambda_Q]\right\}^2 + 4\beta(\beta-1)\cdot \\ \left\{\lambda_Q^2(1-m) - [2(1-q) - \lambda_Q]^2\right\}\left[1 + \lambda_H(2\beta-1)\left(\sqrt{1-m} - 1\right)\right]^2 \end{array}}{4(2\beta-1)^2} = 0 \tag{23}$$

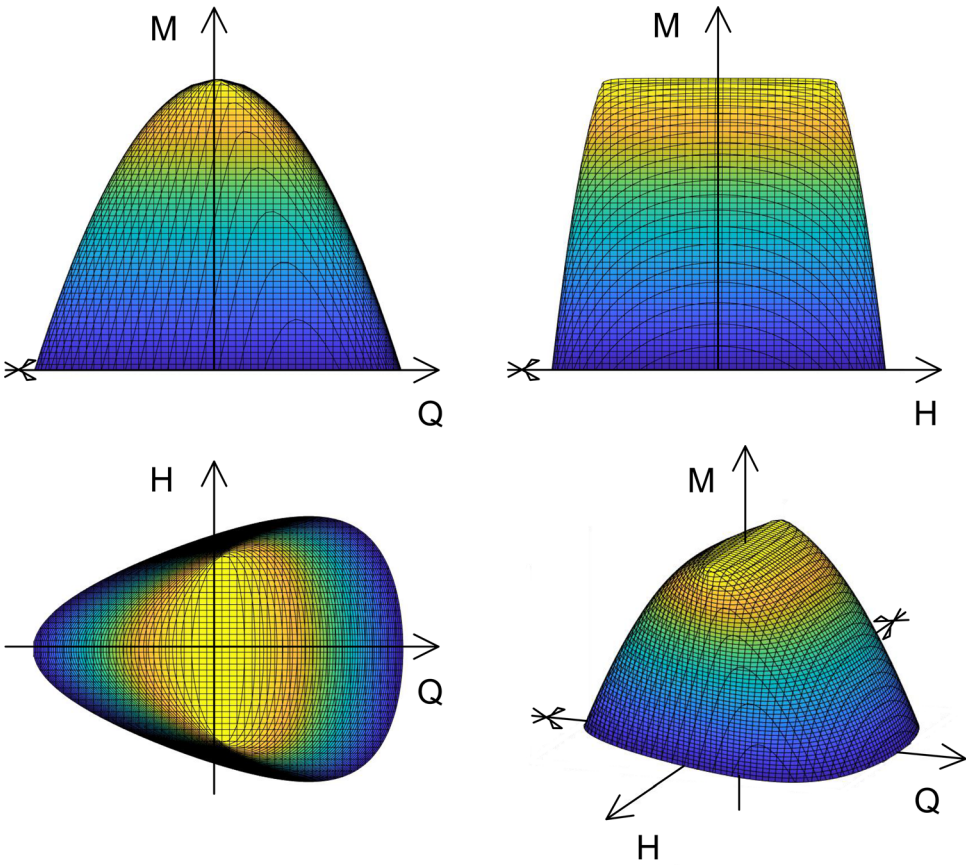

Fig. 5 3D failure surface

where

$$\hat{\boldsymbol{V}} = \begin{Bmatrix} q \\ h \\ m \end{Bmatrix} = \begin{Bmatrix} \dfrac{Q}{Q_c} \\ \dfrac{H}{H_{\max}} \\ \dfrac{M}{M_{\max}} \end{Bmatrix} \tag{24}$$

and

$$\lambda_Q = 1 - \frac{Q_t}{Q_c} \qquad \lambda_H = \frac{i_h R}{H_{\max}} \tag{25}$$

For $H = 0$ and $M = 0$, Eq. (23) reduces, respectively, to:

$$f(\hat{\boldsymbol{V}}) = \lambda_Q^2(1-m) - [2(1-q) - \lambda_Q]^2 = 0 \tag{26}$$

$$f(\hat{\boldsymbol{V}}) = h^2\{\lambda_Q + (2\beta - 1)[2(1-q) - \lambda_Q]\}^2 + 4\beta(\beta - 1)\left\{\lambda_Q^2 - [2(1-q) - \lambda_Q]^2\right\} = 0 \tag{27}$$

The yield surface can be easily derived from Eq. (22),

$$f(\boldsymbol{V}, \rho_c) = \frac{\left[R^2\left(1 - \frac{M}{\rho_c M_{\max}}\right) - \left(\frac{Q}{\rho_c} - b\right)^2\right]\left\{H_{\max} + i_h R(2\beta - 1)\left[\sqrt{1 - \frac{M}{\rho_c M_{\max}}} - 1\right]\right\}^2}{(2\beta - 1)^2} = 0 \tag{28}$$

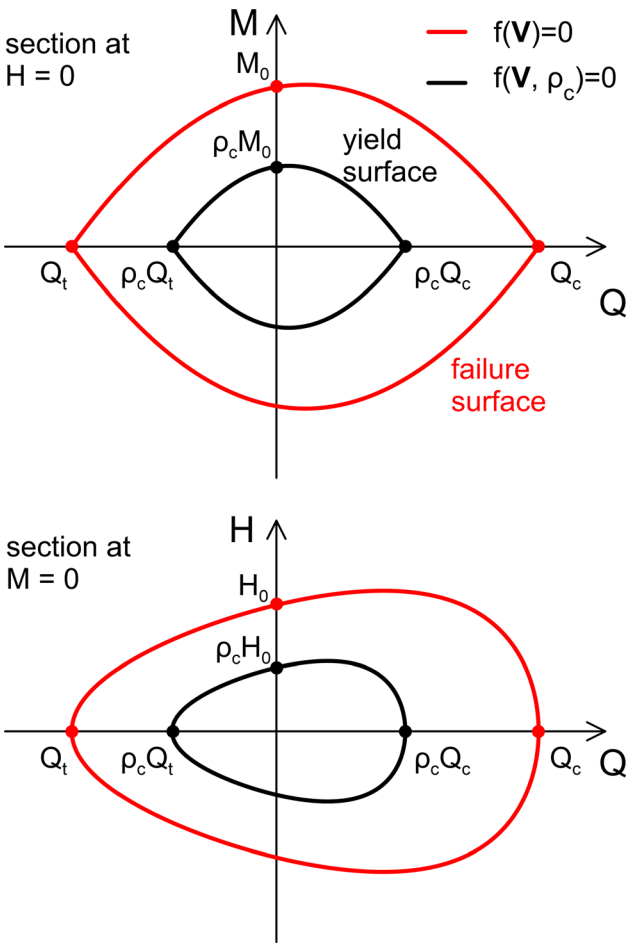

Fig. 6 Failure loci and yield surfaces at $\rho_c = 0.5$ in the (Q, M) and (Q, H) planes

assuming a homothetic relation with centre at the axes origin and ratio ρ_c:

The yield surface for $\rho_c = 0.5$ in either (Q, M) or (Q, H) plane is shown in Fig. 6 together with the failure locus. According to standard concepts in strain-hardening plasticity, the homothetic expansion regulated by ρ_c ends when the current load attains the failure locus. In this situation, only plastic deformations occur as elastic deformations cannot develop any longer.

2.5 Hardening law

A suitable hardening law is constructed herein based on the observed behavior of pile groups under monotonic loading. Specifically, in the case of pure vertical loading, the plastic component of the total displacement can be formulated as:

$$w^p = \frac{Q_c}{K_v} \ln\left(\frac{Q_c}{Q_c - Q}\right) - \frac{Q}{K_v} \tag{29}$$

As Q/Q_c is equal to ρ_c, Eq. (29) can be put in the form:

$$w^p = -\frac{Q_c}{K_v}[\ln(1 - \rho_c) + \rho_c] \tag{30}$$

The generalization to the case of three load components can be obtained by assuming that ρ_c is function of the three plastic displacements, properly weighted:

$$\sqrt{(\alpha_Q\xi)^2+(\alpha_H\eta)^2+(\alpha_M\zeta)^2} = -[\ln(1-\rho_c)+\rho_c] \tag{31}$$

where $(\xi,\eta,\zeta) = \left(\frac{K_v}{Q_c}w^p, \frac{K_h}{H_{max}}u^p, \frac{K_m}{M_{max}B}\theta^p B\right)$ are normalized plastic displacements, while (α_Q, α_H, α_M) are hardening parameters weighting the influence of the different components of the plastic displacement on the evolution of the yield surface. If the elastic component is neglected, $w^p = w$ and Eq. (31) reduces to:

$$\sqrt{(\alpha_Q\xi)^2+(\alpha_H\eta)^2+(\alpha_M\zeta)^2} = -\ln(1-\rho_c) \tag{32}$$

which has the same structure of the hardening law proposed by Nova and Montrasio [28] in the formulation of the rigid-plastic macro-element. The hardening parameters (α_Q, α_H, α_M) in Eq. (32) should be calibrated so as to match the evolution of plastic displacements, as recommended in Nova and Montrasio [28]. As a noteworthy point, they could be not consistent with the reference initial axial, lateral and rotational stiffnesses, as those coming from linear elastic theory or the results of calibration tests. By contrast, in the framework of the proposed model [Eq. (31)], the choice of (α_Q, α_H, α_M) does not affect the initial axial, lateral and rotational stiffnesses of the foundation. Note that this is not a weakness of the model as one could perceive at a first sight; instead, it provides the model with a higher adaptability to reproduce the observed behaviour.

The best option is to calibrate (α_Q, α_H, α_M) against experiments or numerical benchmarks. An example of how this can be achieved is shown hereafter along with some suggestions about their ranges of variation, thus allowing to obtain first approximation prediction of pile group response when data for calibration analysis are not available.

For the sake of completeness, the partial derivatives of Eq. (31), needed to evaluate the plastic multiplier [Eq. (9)] in the proposed model, are reported:

$$\begin{aligned}
\frac{\partial\rho_c}{\partial w^p} &= -\frac{1-\rho_c}{\rho_c[\ln(1-\rho_c)+\rho_c]}\cdot\left(\frac{\alpha_Q K_v}{Q_c}\right)^2|w^p| \\
\frac{\partial\rho_c}{\partial u^p} &= -\frac{1-\rho_c}{\rho_c[\ln(1-\rho_c)+\rho_c]}\cdot\left(\frac{\alpha_H K_h}{H_{max}}\right)^2|u^p| \\
\frac{\partial\rho_c}{\partial \theta^p} &= -\frac{1-\rho_c}{\rho_c[\ln(1-\rho_c)+\rho_c]}\cdot\left(\frac{\alpha_M K_m}{M_{max}B}\right)^2|\theta^p B|
\end{aligned} \tag{33}$$

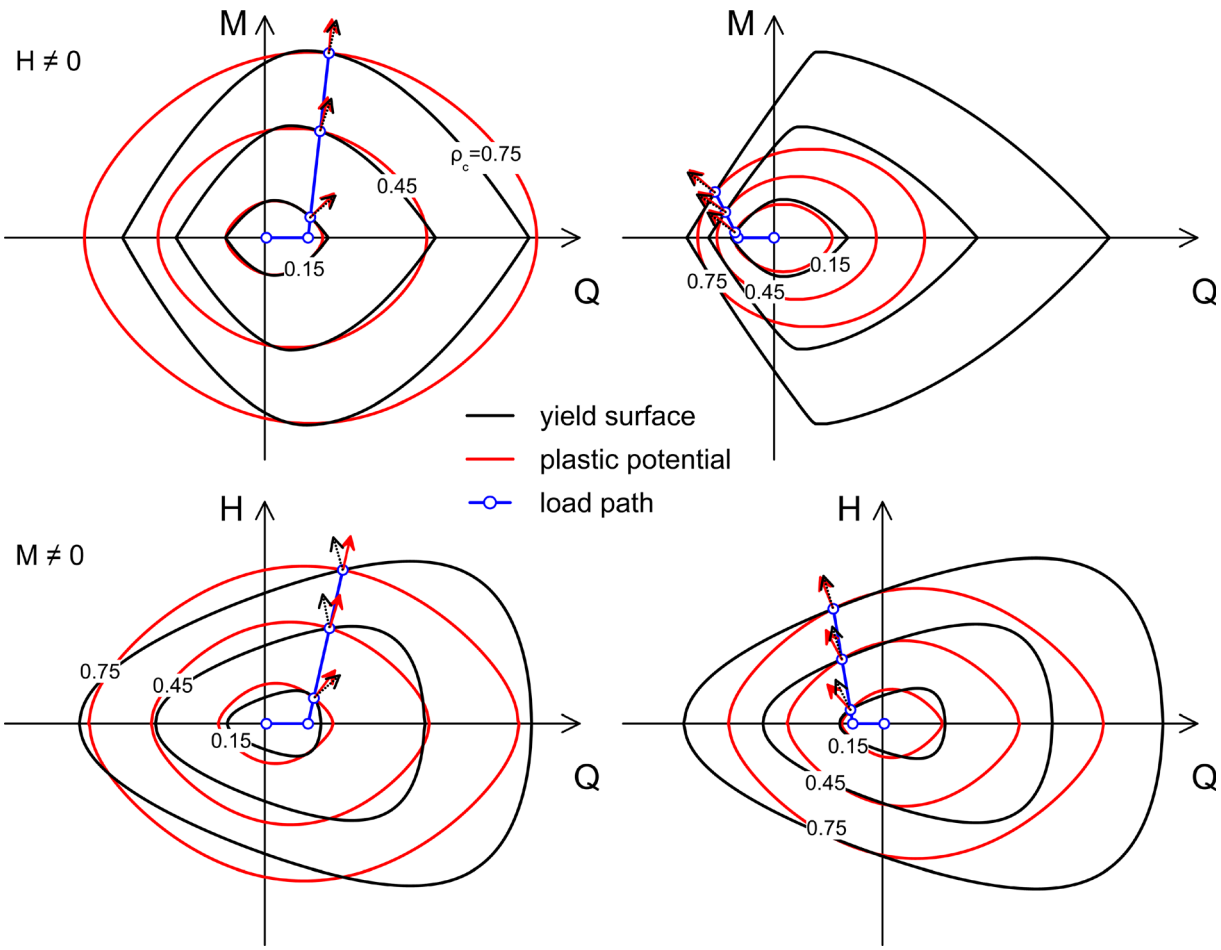

Fig. 7 Flow rule for different loading paths in (Q, M) plane for $H \neq 0$ and in (Q, H) plane for $M \neq 0$

Note that the structure of the mathematical formulation implies that the initial value of memory variable, ρ_{c0}, i.e. the size of the initial elastic region, must be finite.

2.6 Flow rule and plastic potential

The simplest choice for the flow rule in Eq. (7) is to let the plastic potential coincide with the yielding surface (i.e. $f = g$), so that the plastic displacement vector is normal to the yield surface. However, in the case of pile groups this choice does not always lead to realistic results, as detailed in the ensuing (Fig. 7).

With reference to the parabola in the (Q, M) plane for $H = 0$, the current loading state may cross the parabola on the right or left side of the vertex depending on the loading path. In the former case, the direction of the normal to the yielding surface assures that the plastic component of the vertical displacement is directed downward, which is the expected behaviour for pile groups subjected to vertical eccentric load with most of the piles loaded by compressive axial loads. In the latter case, a plastic upward displacement is predicted as it is reasonable at low compression or tensile axial loads owing to the lower stiffness exhibited by the piles subjected to tension, compared to that of piles under compressive loads. It follows that, in principle, the associated flow rule is acceptable in the (Q, M) plane at $H = 0$. Consider now the Granville egg in the (Q, H) plane for $M = 0$. If the yielding function coincides with the plastic potential, the normal to the yielding surface is such that its horizontal component is always directed leftward unless $Q > Q_E$, i.e. for very high axial load level. It follows that the macro-element would generally predict unrealistic upward displacements for an inclined downward force. This issue can be sorted out by using an ad hoc expression for the plastic potential:

$$g(\boldsymbol{V}, \rho_g) = 4\frac{(Q - \rho_g Q_c)(Q - \rho_g Q_t)}{\rho_g^2 (Q_c - Q_t)^2} + \sqrt{\left(\frac{H}{\rho_g H_{\max}}\right)^2 + \left(\frac{M}{\rho_g M_{\max}}\right)^2 + \varepsilon^2} \tag{34}$$

where ρ_g is a scalar parameter allowing the homothetic expansion of the plastic potential with respect to the axes origin and ε is a small, arbitrary and positive quantity (e.g. 10^{-2}) allowing to overcome numerical issues in the calculation of the plastic multiplier when both H and M are equal to 0. Owing to such expansion, for any loading state (Q, H, M) inside the failure locus there always exists a value of ρ_c within]0; 1[satisfying Eq. (31), i.e. there is always a unique yielding surface passing through the current loading state. This is easily understandable thinking of connecting the origin with the current load state through a straight line of length l_1. If this line is extended until reaching the failure surface, a straight line of length l_2 is obtained. The ratio l_1/l_2, which is obviously unique, is the actual value of ρ_c. Following the same rationale, there also exists $\rho_g \neq \rho_c$ which guarantees that the plastic potential passes through the same point (Q, H, M), satisfying Eq. (34).

Note that the plastic potential coincides with the yielding surface only in the (Q, M) plane for $H = 0$ and that its derivatives do not depend on ρ_g.

3 Calibration of ME parameters

The model is characterized by 13 constitutive parameters (Q_c, Q_t, $M_{\max}$, H_c, H_t, K_v, K_h, K_{hm}, K_m, ρ_{c0}, α_Q, α_H, α_M), the majority of which is rather simple to assess and anyhow required in routine design. Concerning the five parameters defining the failure locus, Q_c and Q_t can be easily derived from the axial capacities in compression (N_u) and uplift (S_u) of the isolated pile [e.g., 13, 24], which can be also employed in the approach proposed by Di Laora et al. [8] for the evaluation of $M_{\max}$; H_c and H_t can be calculated from the horizontal capacities of the isolated pile subjected to an axial load equal to N_u and S_u, respectively, as shown in Iovino et al. [22] and Di Laora et al. [9]. The four terms of the elastic stiffness matrix can be determined through simplified expressions in literature or numerical analyses. The value of ρ_{c0} in most common situations may be assumed to be very small (of the order of 10^{-3}, adopted in all subsequent graphs). The most difficult issue is the assessment of the 3 hardening parameters. In principle, the determination of these coefficients would require the availability of benchmarks solutions. In this work, possible ranges for α_Q, α_H and α_M are proposed using data from centrifuge tests in soft clay [7], and from a set of advanced numerical analysis in undrained conditions carried out on small groups of piles under constant axial load [32]. The data from centrifuge tests and numerical analyses served also to assess the performance of the proposed ME in terms of force–displacement curves under inclined and eccentric loads.

3.1 Centrifuge experiments on pile groups under vertical eccentric loads

Reference is made to the centrifuge tests performed at an increased gravity of 50 g on pile groups under eccentric load published by de Sanctis et al. [7], consisting of two series of experiments on annular shaped groups of eight aluminium piles and isolated piles embedded in Speswhite kaolin clay. For the sake of brevity, only the first series of experiments is analysed (set A), including a pile group

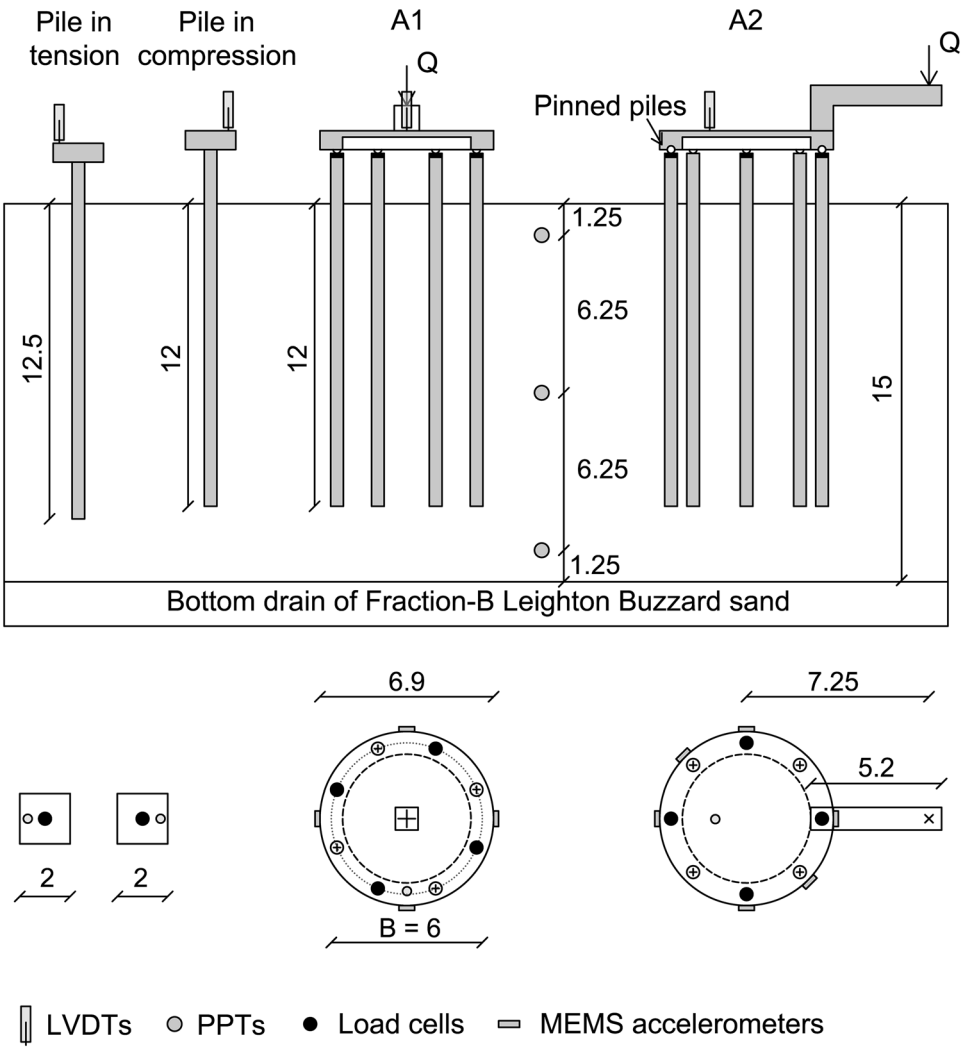

Fig. 8 Plan view and cross-section of the model foundations tested in the centrifuge and soil properties; dimensions (m) are given at prototype scale

Table 1 Failure and elastic parameters of the ME (de Sanctis et al., 2021)

Centrifuge test	Q_c [kN]	Q_t [kN]	M_{max} [kNm]	K_v [MN/m]	K_θ [MNm]
A1 (A2)	2430 (2449)	− 2857 (− 2838)	5648	129	1668

under centred load (*A*1), a pile group under highly eccentric load (*A*2) and two isolated piles, one in compression and one in uplift. The arrangement of the model foundations is schematically depicted in Fig. 8 along with the layout of the recording devices installed to monitor settlements, rotations, axial loads on piles and pore water pressures within the soil mass. Model piles were 1-mm-thick closed-ended hollow cylinders with an outer diameter of 10 mm and an embedded length of 240 mm, coated with a film of Hostun sand. The piles' connection to a circular raft was guaranteed using spherical hinges to allow the piles to carry out only axial loads. The eccentric load on pile group *A*2 was applied by means of a cantilever beam mounted on the raft. For each group, the direction of the load path in the (Q, M) plane is known a priori, allowing an easy identification of the collapse load. As each raft behaves like a rigid body, the settlement of any point belonging to it was evaluated by combining the vertical displacement recorded by the linear variable differential transformer (LVDT) and the rotations derived from the recordings of the micro-electro-mechanical system

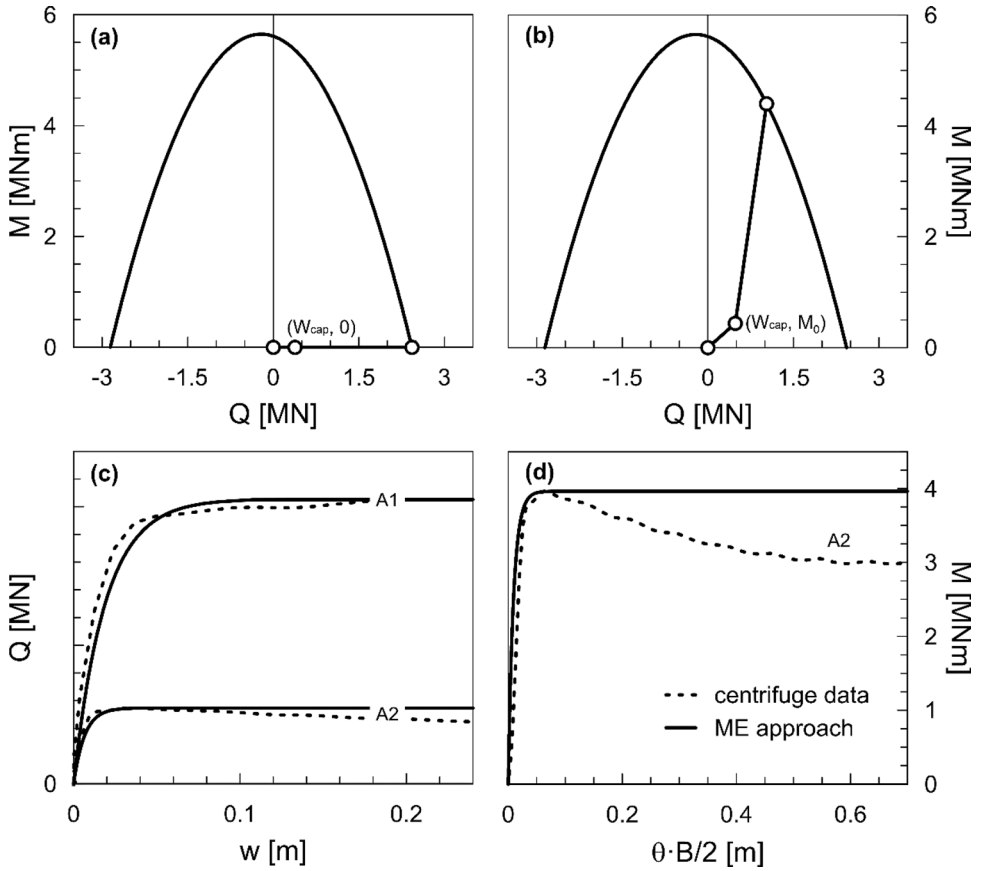

Fig. 9 Failure loci and load paths followed in the centrifuge in tests A1 (**a**) and A2 (**b**). Axial load–settlement curves (**c**) and moment–rotation response (**d**)

(MEMS) accelerometers. Further details can be found in de Sanctis et al. [7]. All data are presented at prototype scale.

Table 1 summarizes the constitutive parameters adopted in the ME analysis for the definition of the failure and yield surfaces and the elastic stiffness matrix, which are derived as detailed in the following. The axial capacity in compression of the pile group, Q_c, is taken directly from test $A1$ subtracting the weight of the piles, W_{piles}, to the failure load coming from the test. The axial capacity in tension, Q_t, is calculated from the test in uplift on the single pile considering an efficiency factor equal to unity and then adding, in absolute terms, the weight of the piles. Note that, since W_{piles} in test $A1$ (834 kN) is slightly larger than in A2 (815 kN), two different set of values of Q_c and Q_t are considered in the two ME simulations. The maximum value of the moment capacity, M_{max}, is calculated as the vertex of the parabola passing through the points (Q_c, 0), (Q_t, 0), (Q_{A2}, M_{A2}), where Q_{A2} and M_{A2} are the coordinates of the endpoint of the load path followed in test $A2$. The vertical and rotational stiffnesses of the pile group, K_v and K_θ, are calculated from the initial axial stiffness of the isolated pile, K_s, which was estimated to be 45 MN/m, using superposition and modelling pile-to-pile interaction effect with the approximate solution by Dobry and Gazetas [11] as in Iovino et al. [23].

The failure loci of the model foundations $A1$ and $A2$, along with the loading paths followed in the centrifuge, are plotted in Fig. 9a and b, respectively. Note that, because of symmetry, only half of the collapse domain is plotted. Moreover, the load paths only refer to the external load on the pile group and do not include the weight of the piles, W_{piles}, which was not considered in the analysis. The first point of each path is the preload on the foundation due to the weight of the cap, W_{cap}. For pile group $A2$, this point has a positive ordinate, M_0, corresponding to the moment due to the weight of the cantilever beam used to apply the external eccentric load. Notably, experimental data do not include the displacement due to W_{cap}.

The axial response determined experimentally from test $A1$ is compared to that evaluated through the ME in Fig. 9c under the assumption $\alpha_Q = 1$.

The prediction of the proposed model satisfactorily matches the observed behaviour, so that $\alpha_Q = 1$ is also taken for the simulation of test $A2$. The axial load–settlement, Q–w, and moment–rotation, M–θ, curves predicted using (α_Q, α_M) = (1, 1) are compared to those gathered

Table 2 Failure and elastic parameters of the ME

Pile group	Q_c [MN]	Q_t [MN]	M_{max} [MNm]	H_c [MN]	H_t [MN]	K_v [MN/m]	K_h [MN/m]	K_{hm} [MN]	K_m [MNm]
2 × 1	8.48	− 7.07	11.66	4.15	0.15	2.34	0.76	1.51	8.44
3 × 1	12.72	− 10.60	23.33	6.23	0.23	3.16	0.98	28.61	3.07
4 × 1	16.96	− 14.14	46.65	8.31	0.31	3.98	1.18	63.26	4.92

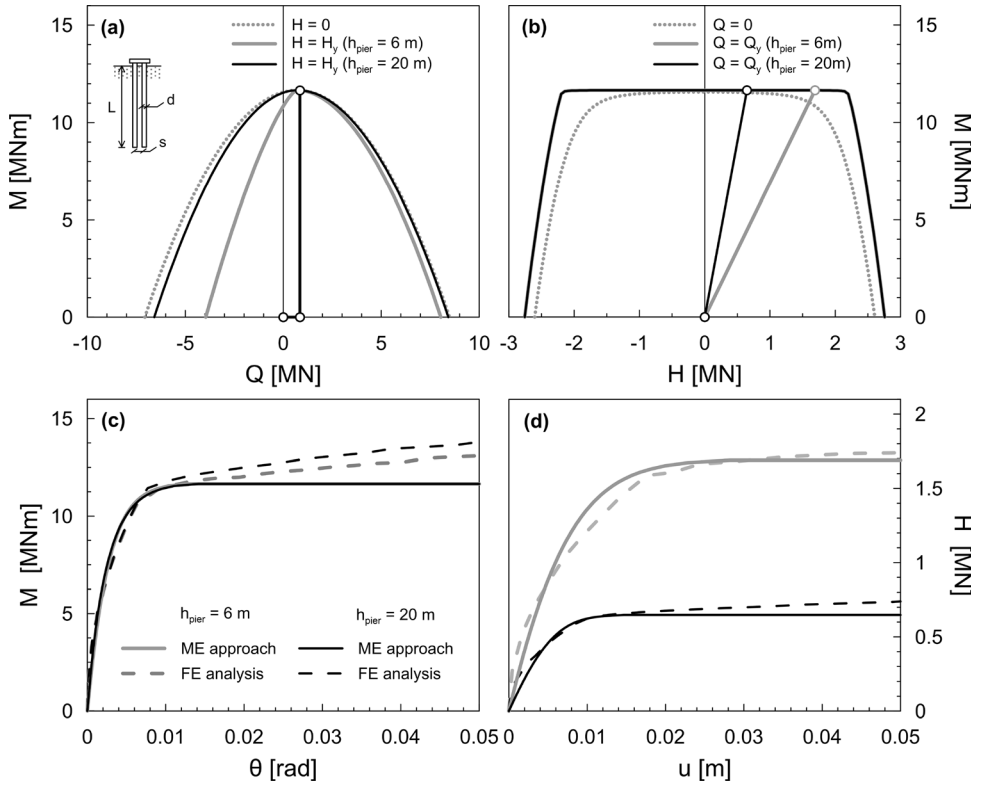

Fig. 10 (2 × 1) pile group under FS_v = 10: load path and failure loci in the (Q, M) and (H, M) planes (**a**, **b**); moment–rotation curves (**c**); lateral load–deflection curves (**d**)

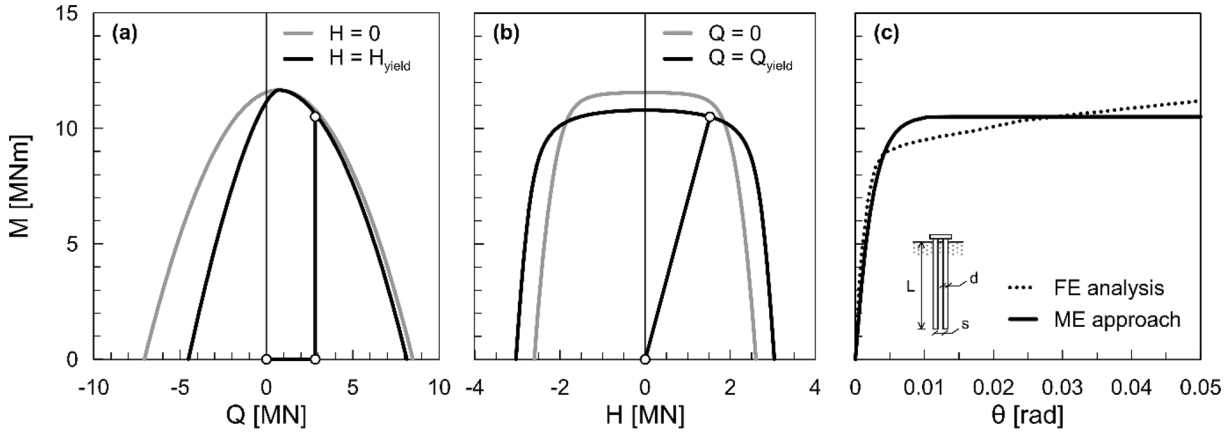

Fig. 11 (2 × 1) pile group under FS_v = 3: load path and failure loci in the (Q, M) and (H, M) planes (**a**, **b**); moment–rotation curves (**c**)

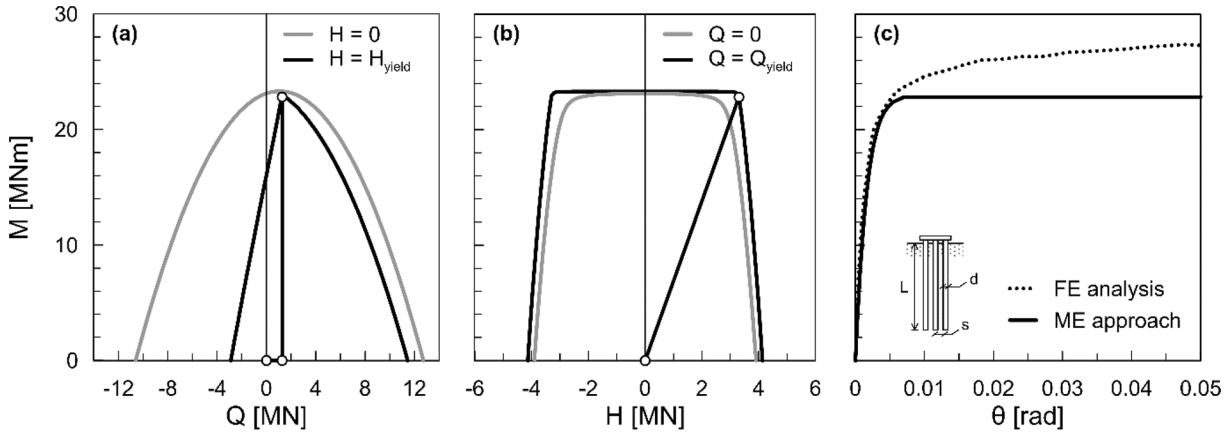

Fig. 12 (3 × 1) pile group under $FS_v = 10$: load path and failure loci in the (Q, M) and (H, M) planes (**a**, **b**); moment–rotation curves (**c**)

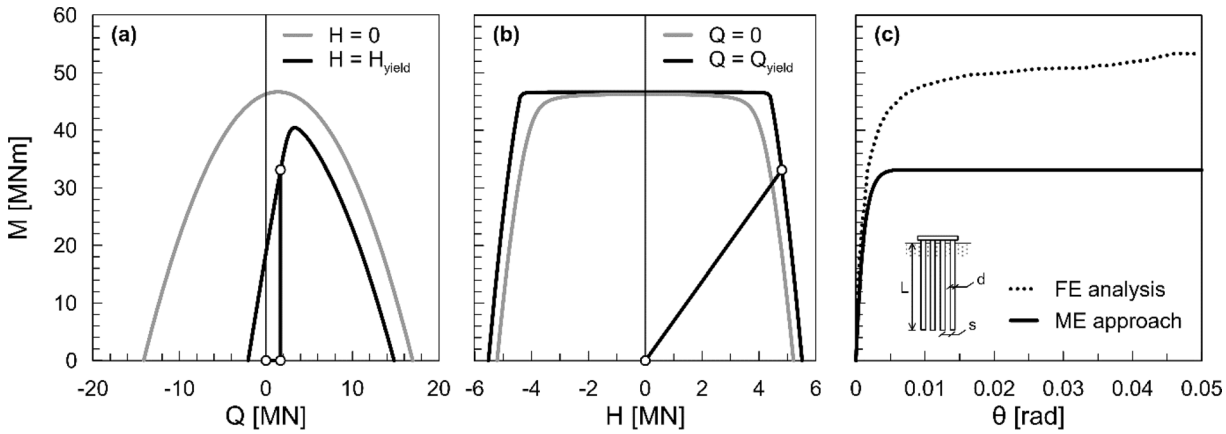

Fig. 13 (4 × 1) pile group under $FS_v = 10$: load path and failure loci in the (Q, M) and (H, M) planes (**a**, **b**); moment–rotation curves (**c**)

from test *A*2 in Fig. 9c and d, respectively, in which B is the diameter of the circle passing through the centres of the piles. Also for test *A*2 the obtained results are in very good agreement with the experimental data in terms of both rotational and translational response.

3.2 Numerical analyses of pile groups under inclined eccentric loads

In this section, the ME is calibrated and validated against the results of FE analyses on small groups of piles in clay subjected to inclined and eccentric loads performed by Psychari and Anastasopoulos [32]. Three groups of (2 × 1), (3 × 1) and (4 × 1) piles are first loaded vertically and then subjected to a horizontal load applied under constant eccentricity represented by the pier height, $h_{pier} = 6$ m or 20 m. Different load paths are followed by varying the amount of the axial load and the eccentricity of the lateral action. An idealized, homogeneous clay deposit with uniform undrained shear strength $s_u = 100$ kPa is considered. The soil behaviour is modelled with a kinematic hardening model with von Mises failure criterion and associated flow rule, while reinforced concrete (RC) piles are idealized by a combination of nonlinear continuum elements for the concrete and surface elements for the longitudinal reinforcement so as to simulate the dependence of the plastic yielding moment of the pile cross-section, M_y, from the axial load, N.

To investigate in detail the mechanism of interaction under combined loads, Psychari and Anastasopoulos [32] distinguish between the moment component due to the axial resistance of the piles and that associated with the flexural strength of the concrete cross-section, referred to in the original work as M_{ax} and M_b, respectively. In order to make the ME outcome comparable to the FE simulations, the focus is set only on the first contribution.

The axial capacities in compression, Q_c, and tension, Q_t, of each pile group are evaluated from the axial capacities of the isolated pile, N_u and S_u, determined by the authors employing analytical solutions. An efficiency factor of unity is adopted. The moment capacity of the group, M_{max}, is calculated from N_u and S_u, using the solution by Di Laora

et al. [8]. Considering the layout of the longitudinal reinforcement and the material properties of the RC piles, the horizontal capacities of the single pile are first estimated applying the Broms [2] theory for fixed head piles in clay under N_u or S_u; then, the horizontal capacities of the group, H_c, and H_t, are obtained postulating an efficiency factor under horizontal load equal to unity.

The complete stiffness matrix is established from the code Dynapile (Ensoft) based on the consistency boundary matrix method [1] by setting the excitation frequency at zero. The parameters of the ME are resumed in Table 2 for each foundation, except those pertinent to the hardening law which were determined with the following approach. Since in the reference numerical analyses data on vertical displacements were not available, the hardening parameter α_Q is assumed to be unity, in line with what was accomplished after the calibration analysis performed for test $A1$. The remaining hardening parameters (α_H, α_M) are backfigured from the numerical test carried out on the (2 × 1) pile group with a vertical safety factor $FS_v = 10$ and the 6 m high pier. The load path and the corresponding moment-rotation and horizontal load–deflection curves are shown in Fig. 10 for (α_H, α_M) = (0.5, 0.5). It is evident that this choice allows for a very satisfactory prediction of the pile group response. All subsequent analyses must thus be intended for validation.

The ME outcome for the (2 × 1) pile group under lateral load with larger eccentricity, i.e. $h_{pier} = 20$ m (Fig. 10), also matches in a satisfactory way the data gathered from the FE analysis.

Figure 11 illustrates the comparison between the ME and the FE analysis by Psychari and Anastasopoulos [32] for $h_{pier} = 6$ m and $FS_v = 3$, that is at an axial load far larger than before. Data about lateral deflection were not available in this case, so that the comparison is limited to the moment–rotation curve. Even though the ME is unable to grasp the hardening response predicted by the FE model at very large rotations, the response predicted matches quite satisfactorily the reference solution.

Finally, the performance of the ME is investigated for the (3 × 1) and (4 × 1) layouts in Figs. 12 and 13, respectively. Data are available for these two foundations only in terms of cap rotations and the model pier 6 m high. The agreement is quite reasonable for the (3 × 1) pile group, while there is a significant difference between the two plots for the layout with four piles. However, this is due to the increase of shaft capacity of the piles in the group owing to action of the lateral load, a 3D effect that cannot be simulated using the ME approach.

The successful comparison with the numerical analysis carried out employing an advanced constitutive model indicates the potential of the proposed ME over time-consuming FE analyses.

4 Conclusions

A new macro-element model for pile groups subjected to monotonic loads, developed in the framework of strain hardening elasto-plasticity, has been presented and discussed. The basic assumption, realistic for small pile groups, is that the piles' connecting cap behaves like a rigid body, that is to assume only three kinematic variables (u, w, θ) as representative of the foundation response. The closed-form equation of the failure locus of the foundation is among the novel contributions of this work and can also be conveniently employed for ultimate limit state analysis of a pile group when subjected to multi-component loads. A generalized hardening law is formulated as an extension of the equation originally suggested by Nova and Montrasio [28] for shallow foundations, while a new expression for the plastic potential is introduced to allow the use of non-associative plastic flow rule. In addition to this, the proposed model considers also the recoverable part of displacements.

The ME requires a few parameters, most of which are already needed in routine design. The main difficulty is the calibration of the hardening coefficients for which possible ranges are provided for piles in either soft or heavily overconsolidated clays. The ability of the ME in predicting the behaviour of pile groups subjected to monotonic loads has been checked against data from centrifuge tests and rigorous numerical analyses, providing good performance. While the model is very successful in capturing the general patterns of the behaviour in combined loading, it is unable to predict the hardening of the moment–rotation response under eccentric lateral load at very large displacements, that is, however, a problem of minor engineering concern and anyhow out of the main scope of the model.

Acknowledgements This work has been carried out under research project MIUR PRIN 2017 'A new macro-element model for pile groups under monotonic, cyclic and dynamic loadings' granted by the Italian Ministry for Research and University. The authors would like to thank Prof. Claudio Tamagnini from University of Perugia and Dr. Luca Flessati from University of Delft for the stimulating discussion on the subject.

Funding Open access funding provided by Università degli Studi della Campania Luigi Vanvitelli within the CRUI-CARE Agreement.

References

1. Blaney GW, Kausel E, Roesset JM (1976) Dynamic stiffness of piles. In: Proceedings of second international conference on numerical methods in geomechanics. ASCE Blacksburg, Virginia, pp 1001–1012
2. Broms BB (1964) Lateral resistance of piles in cohesive soils. J Soil Mech Found Div 90(2):27–63
3. Butterfield R, Banerjee PK (1971) The problem of pile group–pile cap interaction. Géotechnique 21(2):135–142
4. Cassidy MJ, Byrne BW, Randolph MF (2004) A comparison of the combined load behaviour of spudcan and caisson foundations on soft normally consolidated clay. Géotechnique 54(2):91–106
5. Cassidy MJ, Randolph MF, Byrne BW (2006) A plasticity model describing caisson behaviour in clay. Appl Ocean Res 28(5):345–358
6. Chatzigogos CT, Pecker A, Salencon J (2009) Macroelement modeling of shallow foundations. Soil Dyn Earthq Eng 29(5):765–781
7. de Sanctis L, Di Laora R, Garala TK, Madabhushi SPG, Viggiani GMB, Fargnoli P (2021) Centrifuge modelling of the behaviour of pile groups under vertical eccentric load. Soils Found 61(2):465–479
8. Di Laora R, de Sanctis L, Aversa S (2019) Bearing capacity of pile groups under vertical eccentric load. Acta Geotech 14(1):193–205
9. Di Laora R, Iodice C, Mandolini A (2022) A closed-form solution for the failure interaction diagrams of pile groups subjected to inclined eccentric load. Acta Geotech 17(8):3633–3646
10. Di Prisco C, Nova R, Sibilia A (2002) Analysis of soil-structure interaction of towers under cyclic loading. In: Pande GN, Pietruszczak S (eds) Numerical models in geomechanics – NUMOG VIII, invited lecture, proceedings of NUMOG 8. Swets & Zeitlinger, Lisse, pp 637–642
11. Dobry R, Gazetas G (1988) Simple method for dynamic stiffness and damping of floating pile groups. Géotechnique 38(4):557–574
12. Figini R, Paolucci R, Chatzigogos CT (2012) A macro-element model for non-linear soil–shallow foundation–structure interaction under seismic loads: theoretical development and experimental validation on large scale tests. Earthq Eng Struct Dyn 41(3):475–493
13. Fleming K, Weltman A, Randolph M, Elson K (2008) Piling engineering. CRC Press
14. Foglia A, Gottardi G, Govoni L, Ibsen LB (2015) Modelling the drained response of bucket foundations for offshore wind turbines under general monotonic and cyclic loading. Appl Ocean Res 52:80–91
15. Gerolymos N, Papakyriakopoulos O (2016) Macroelement modelling of laterally loaded piles and pile-groups. In 1stInt. Conf. On natural hazards and infrastructure, ICONHIC
16. Gorini DN, Callisto L (2022) Generalised ultimate loads for pile groups. Acta Geotech 17(6):2495–2516
17. Gorini DN, Callisto L (2023) A multiaxial inertial macroelement for deep foundations. Comput Geotech 155:105222
18. Gottardi G, Houlsby GT, Butterfield R (1999) Plastic response of circular footings on sand under general planar loading. Géotechnique 49(4):453–469
19. Grange S, Kotronis P, Mazars J (2008) A macro-element for a circular foundation to simulate 3D soil–structure interaction. Int J Numer Anal Methods Geomech 32(10):1205–1227
20. Houlsby GT, Cassidy MJ (2002) A plasticity model for the behaviour of footings on sand under combined loading. Géotechnique 52(2):117–129
21. Iodice C, Iovino M, Di Laora R, de Sanctis L, Mandolini A (2023) A macro-element for pile groups subjected to vertical eccentric load. In: National conference of the researchers of geotechnical engineering. Springer Nature Switzerland, Cham, 210–217
22. Iovino M, de Sanctis L, Maiorano RMS, Aversa S (2021) Failure envelopes of pile groups under inclined eccentric load. Géotech Lett. https://doi.org/10.1680/jgele.21.00059
23. Iovino M, Di Laora R, de Sanctis L (2021) Serviceability limit state analysis of piled foundations under combined axial-moment loading. Acta Geotech 16(12):3963–3973
24. Letizia N, Iodice C, Mandolini A (2018) A local design method for pile foundations. Advances in Civil Engineering
25. Li Z, Kotronis P, Escoffier S, Tamagnini C (2016) A hypoplastic macroelement for single vertical piles in sand subject to three-dimensional loading conditions. Acta Geotech 11:373–390
26. Marchi M, Butterfield R, Gottardi G, Lancellotta R (2011) Stability and strength analysis of leaning towers. Géotechnique 61(12):1069–1079
27. Martin CM, Houlsby GT (2001) Combined loading of spudcan foundations on clay: numerical modelling. Géotechnique 51(8):687–699
28. Nova R, Montrasio L (1991) Settlements of shallow foundations on sand. Géotechnique 41(2):243–256
29. Pender M, Wotherspoon L, Sa'Don NM, Orense R (2011) Macro element for pile head cyclic lateral loading. In: Sakr MA, Ansal A (eds) Special topics in earthquake geotechnical engineering. Springer Netherlands, Dordrecht, pp 129–145
30. Pisanò F, Di Prisco C, Lancellotta R (2014) Soil–foundation modelling in laterally loaded historical towers. Géotechnique 64(1):1–15
31. Poulos HG (1968) The behaviour of a rigid circular plate resting on a finite elastic layer. Civ Eng Trans 10:213–219
32. Psychari A, Anastasopoulos I (2022) Combined loading of RC pile groups in clay accounting for N–M interaction. Soil Dyn Earthq Eng 163:107490
33. Roscoe KH, Schofield AN (1957) The stability of short pier foundations in sand. Br Weld J 4:343–354
34. Salciarini D, Tamagnini C (2009) A hypoplastic macroelement model for shallow foundations under monotonic and cyclic loads. Acta Geotech 4:163–176
35. Schotman GJM (1989) The effects of displacements on the stability of jackup spud-can foundations. In: Offshore technology conference. OnePetro